Towards Perpetual Flight of a Gliding Unmanned Aerial Vehicle in the Jet Stream

Joachim L. Grenestedt and John R. Spletzer, *Member, IEEE*

***Abstract*—In this paper, we investigate the potential of a self-powered gliding aircraft to remain aloft indefinitely. We focus specifically on operations in the jet stream where persistent wind gradients can be used to enable unpowered flight. The advantage of such a paradigm is that power requirements are reduced to those needed for aircraft navigation, control, and communication systems. To investigate the feasibility of such an approach, we examine both aircraft design requirements for perpetual flight, as well as trajectory strategies for solar power generation. Both the aircraft design and power generation problems are cast as non-linear optimization problems where the aircraft equations of motion and periodicity serve as constraints to ensure that sustainable flight trajectories are maintained. Simulation results indicate a suitable aircraft design capable of unpowered flight in the jet stream and capable of generating sufficient electrical power can be achieved.**

I. Introduction & Related Work

Despite great strides from decades of research and development, there are still significant costs and risks associated with placing satellites into orbit. In 2009 alone, 5 of 78 space launches ended in failure [1]. In contrast, a self-powered aircraft capable of remaining aloft indefinitely would allow low altitude/cost satellite systems to be put into place, recovered, and maintained without the significant expense and failure risk associated with space launch. This has significant implications to applications such as communications, surveillance, and weather monitoring to name but a few.

It should come as no surprise then that the idea of perpetual flight has been an active research area for several decades. The bulk of this work has focused on solar powered flight [2]. Recent relevant results includes the work of AC Propulsion, which demonstrated multi-day solar-powered flight with their SoLong UAV [3]. Noth *et al* developed an ultra-light solar powered UAV which achieved flights over 24 hours in duration [4]. Klesh and Kabamba looked at path planning techniques to maximize energy for perpetual flight of a propeller powered aircraft [5]. More ambitious efforts include the DARPA Vulture project to develop an aircraft that can remain on station for 5 years [6], and the Solar Impulse group that is developing a manned solar powered aircraft capable of autonomous takeoff and flying for an around-the-world flight with a planned launch date in 2011 [7]. Each of these efforts share a common theme in that motive power for the aircraft is provided via solar energy generated in-flight. However, there are significant challenges associated with solar-powered aircraft. These include fragility and difficulties in control due to the very long wings needed for minimum propulsive power, as well as sufficient surface area for mounting the solar arrays. Instead, we pursue a different approach. Specifically, we are interested in vehicles capable of unpowered flight, *i.e.,* gliding aircraft, through dynamic soaring.

Dynamic soaring is a technique whereby horizontal wind that varies in strength or direction is used to support flight. Rayleigh is usually accredited for first suggesting that soaring can be done in a horizontal but non-uniform wind field [8]. Seabirds like albatrosses are known to travel hundreds of kilometers in a single day utilizing dynamic soaring [9]. Save for an anecdote of a flight in Australia in 1974, attempts for sustained dynamic soaring of manned gliders appear to not have been fully successful as of yet. However, radio controlled hobby aircraft routinely dynamically soar in the steep wind gradients on the leeward side of mountain ridges, and have reached speeds over 600 km/h. In this paper, we limit our focus to dynamically soaring aircraft operating in the jet stream. Jet streams are bands of strong winds in the upper atmosphere that extend for 1000s of kilometers, but are relatively narrow (< 5 km thick) [23]. Unlike locations that are dependent upon surface winds, the gradients in the jet stream are persistent and have the potential to support perpetual flight.

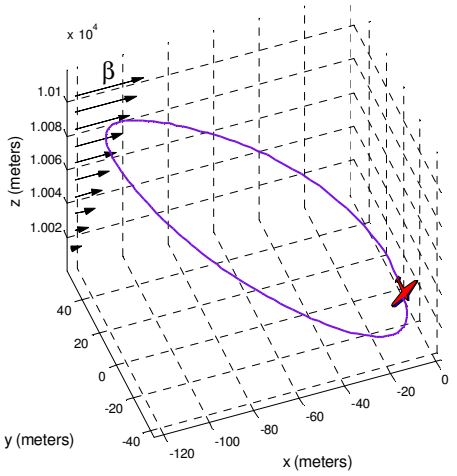

Figure 1: A dynamic soaring trajectory for loitering. The aircraft climbs into the wind gradient β to gain altitude, and dives with the wind to gain velocity. The energy obtained from such a trajectory can support perpetual flight.

An example of a dynamic soaring trajectory is shown at Figure 1. In this example, the aircraft assumes a loitering behavior whereby the start and end positions of the

J. Grenestedt is with the Department of Mechanical Engineering and Mechanics, Lehigh University, Bethlehem, PA, 18015, USA (corresponding author, e-mail: jog5@ lehigh.edu).

J. Spletzer is with the Department of Computer Science and Engineering, Lehigh University, Bethlehem, PA, 18015, USA.

trajectory are the same. The general strategy for dynamic soaring is for the aircraft to climb into the wind gradient β (exaggerated for illustration purposes) in order to gain altitude, and then dive with the wind to gain velocity. Under appropriate conditions, the energy gained from such a trajectory can support perpetual flight. A number of papers have been devoted to optimizing trajectories of dynamically soaring aircraft, flying either in near-ground wind gradients or in wind gradients associated with high altitude jet streams. These include the works of Boslough [10], Zhao [11], Sachs and da Costa [12], Gordon [13], Akhtar *et al* [14], and Lawrance and Sukkarieh [15-16]. Deittert *et al* looked at the dynamic soaring problem using differential flatness to transform the optimization problem [25]. Perhaps most related to our work is [12], where the authors investigated the problem of finding the smallest wind gradient that would sustain flight for a given aircraft design. Their results indicated that soaring in vertical wind gradients associated with the jet stream (*i.e.,* 0.01-0.02 s^{-1}) was feasible for a specific set of aircraft parameters.

While soaring mitigates the need for providing motive power to the aircraft, onboard navigation, control and communications systems still require power. In this paper, we build upon these results to examine both aspects of the perpetual flight problem. We first develop an aircraft model that is parameterized by a compact set of aircraft engineering design variables. We then pose the dynamic soaring problem as a non-linear optimization problem whereby the equations of motion and control inputs are modeled as nonlinear constraints to ensure a periodic soaring trajectory is achieved. Using this formulation, we are able to solve for our aircraft design parameters to develop a realistic aircraft capable of dynamic soaring. We then develop flight trajectories for this aircraft which optimize the amount of power that can be recovered from on-board solar cell arrays. The net result is a more realistic aircraft design, and flight trajectories capable of supporting perpetual flight.

II. THE AIRCRAFT MODEL

As our initial results presented herein will be limited to simulations, we desired a reasonably realistic aircraft model for validation purposes while still maintaining a relatively compact set of design parameters. To this end, we chose wing span b, wing area S_w, fuselage length l, and aircraft mass m as our design parameters. Other design variables were either dependent upon these parameters or were fixed based upon heuristics. The derivation of our aircraft model follows.

To estimate the drag over the wing, the coefficient of drag for the NACA 634132 airfoil versus Reynold's number R in the range of 100,000 to 9,000,000 was used. The data are in reasonably close agreement to what would be estimated by Schoenherr's formula,

$$c_d^w = 2.0 \cdot C_f \tag{1}$$

where the factor 2.0 approximates the wet area (or circumference) of the airfoil and C_f is the turbulent skin drag coefficient which can be estimated from Schoenherr's formula [24]. We assumed that the zero-lift (parasitic) drag from the wing and tail surfaces was

$$D_0^w = 1.5 c_d^w S_w q \tag{2}$$

where $q=\rho V^2/2$ is the dynamic pressure from air with density ρ and velocity V, and the factor 1.5 accounted for the vertical and horizontal stabilizers (their size may be 20% each of the wings, but they have lower Reynold's numbers). Based upon general aircraft design heuristics, we assumed a horizontal stabilizer area S_h that was 20% of the wing area S_w, and a stabilizer volume $S_h l_h$ of 40% of the wing volume $S_w c_w$. The vertical tail volume $S_v l_v$ was modeled as 4% of the wing volume $S_w b$. Assuming the tail arms are the same, $l_h=l_f$, and the vertical tail has the same area as the horizontal tail, $S_f=S_h=0.2S_w$, then these requirements reduce to

$$l_h = l_v \geq \max(2c_w, 0.2b) = \max(2S_w / b, 0.2b) \tag{3}$$

and the total length of the fuselage is

$$l = 2c_W + l_h \geq 2S_w / b + \max(2S_w / b, 0.2b) \tag{4}$$

where c_w is the wing chord length. Note that although fuselage length is a design parameter, this implies a lower bound for l as a function of the aircraft wing area and wing span. For a streamlined fuselage with an essentially round cross section, the wet area was estimated by

$$S^f = 0.75\pi d_f l \tag{5}$$

where d_f is the maximum diameter of the fuselage. The drag of the fuselage can then be estimated as

$$D_0^f = 1.25 C_f S^f q \approx \frac{0.9\pi d_f l q}{(3.46 \log R^f - 5.6)^2} \tag{6}$$

where R^f is the fuselage Reynold's number, and the 1.25 factor accounted for the thickness of the fuselage. The total parasitic drag of the aircraft can be written as

$$\begin{aligned} D_0 = D_0^w + D_0^f &= 1.5 \cdot 2.0 \cdot C_f^w S q + 1.25 \cdot C_f^f S^f q \\ &\approx \frac{3 S_w q}{(3.46 \log R^w - 5.6)^2} + \frac{0.9\pi d l q}{(3.46 \log R^f - 5.6)^2} \end{aligned} \tag{7}$$

Note that different Reynold's numbers need to be used for the wing and the fuselage

$$R^w = \frac{V c_w}{\nu}, \quad R^f = \frac{V l}{\nu} \tag{8}$$

where ν is the kinematic viscosity of air.

A lower bound on the mass m of the aircraft can be determined from the sum of the masses of the wing skins m_{skin}, the wing spar m_{spar}, the fuselage m_f, and a fixed mass m_0 for the avionics, batteries, *etc.* It is difficult to make a wing skin that can be handled without damage with less than 150 g/m^2 carbon fiber for each skin of a sandwich with a 4 mm honeycomb core. The mass of the carbon fiber composite is 150/0.63=238 g/m^2 if the matrix mass fraction is 37%. The mass of a 4 mm thick 48 kg/m^3 Nomex

honeycomb is 192 g/m^2. For sufficient bonding strength a 100 g/m^2 glue film may be required. The total mass is then 2·(238+100)+192=870 g/m^2=0.87 kg/m^2. This applies to top and bottom wing and stabilizer skins. The total wing and stabilizer skin mass is thus approximately (using planform areas and assuming that the stabilizer areas are 20% each of the wing area)

$$m_{skin} = 0.87 \cdot 2 \cdot 1.4 S_w = 2.44 S_w \tag{9}$$

If the airfoil thickness was 12%, then the thickness d of the wing spar may be 10%.

$$d = 0.1 c_w = \frac{0.1 S_w}{b} \tag{10}$$

The maximum wing bending moment M is approximately

$$M = \frac{Nmgb}{8} \tag{11}$$

where N is the largest load factor. The stress in the spar caps is approximately

$$\sigma = \frac{M}{twd} \tag{12}$$

where t is the thickness and w the width of the spar cap. With an allowable stress (in compression) of σ_a, the minimum spar cap area becomes

$$tw = \frac{M}{\sigma_a d} = \frac{Nmgb}{8\sigma_a d} \tag{13}$$

where m is again the total mass of the aircraft. Assuming that this is twice the average spar cap area, and that the top and bottom spar caps are identical, the mass of the spar caps can be estimated,

$$m_{cap} = twb\rho_{cfrp} = \frac{Nmgb^2 \rho_{cfrp}}{8\sigma_a d} = \frac{Nmgb^3 \rho_{cfrp}}{0.8\sigma_a S_w} \tag{14}$$

Reasonable values for carbon fiber are ρ_{cfrp}=1,550 kg/m^3, σ_a=700 MPa, and with N=10 we obtained

$$m_{cap} = 2.7 \cdot 10^{-4} \frac{mb^3}{S_w} \tag{15}$$

We assumed that the total mass of the wing spar was ≈50% above this, *i.e.*,

$$m_{spar} = 4 \cdot 10^{-4} \frac{mb^3}{S_w} \tag{16}$$

For a relatively small aircraft, the fuselage skins can be assumed to be made like the wing skins with a mass of 0.87 kg/m^2. For this work, we assumed the maximum fuselage diameter d_f = 0.1 meters, so the mass of the fuselage skins was

$$m_f = 0.87 \cdot 0.75\pi d_f l \approx 0.2l \tag{17}$$

A lower bound for the total mass of the aircraft was then

$$m \geq m_{skin} + m_{spar} + m_f + m_0 = \frac{2.44 S_w + 0.2l + m_0}{1 - 4 \cdot 10^{-4} b^3 / S_w} \tag{18}$$

Note that in practice, a higher mass may in fact be desirable to achieve optimal dynamic soaring behavior. This will be revisited in Section V.

III. SOLAR RADIATION MODEL

While motive power for the aircraft will not be required, electricity is still needed for on-board avionics, control systems, *etc.* To this end, we assume that electrical power will be provided through batteries that are recharged daily by an integrated solar cell array. To estimate the solar irradiance as witnessed by the aircraft – and implicitly the power that can be generated – a clear-sky solar radiation model was used based upon the work of [17]-[20]. This is an appropriate model for the altitudes at which we will be operating This model traditionally integrates contributions from beam, diffuse, and reflected radiation. Under clear sky conditions, beam radiation predominates. This is especially true at the altitudes we propose to operate (≈10km above mean sea level), as most of the scattering effects that contribute to atmospheric turbidity and Rayleigh scattering occur within a few kilometers of the earth's surface. As such, we examine only the effect of beam irradiance for generating power, with the understanding that our results will at worst be conservative.

The irradiance B normal to the solar beam can be estimated by

$$B = G_0 \exp[-0.8662 \cdot T_{LK} \cdot m_{air} \cdot D_R(m_{air})] \tag{19}$$

where G_0 is the solar constant normalized to take into account the annual variation of the sun-earth distance, T_{LK} is the Linke turbidity factor, and

$$m_{air} = \frac{p / p_0}{\sin\theta_{ref} + 0.50572 (\theta_{ref} + 6.07995)^{-1.6364}} \tag{20}$$

is the relative optical air mass through which the beam has traveled, where θ_{ref} is the corrected solar altitude (in degrees) to account for atmospheric refraction and

$$p / p_0 = \exp(-z / 8434.5) \tag{21}$$

is a correction for aircraft altitude z (in meters), and

$$D_R(m) = \frac{10000}{66296 + 17513m - 1202m^2 + 65m^3 - 1.3m^4} \tag{22}$$

is the optical depth from Rayleigh scattering as a function of the air mass. This is the same model used in [21].

As the anticipated duration of a periodic soaring cycle is relatively short (on the order of a minute), we assumed that the solar altitude (θ_s) and azimuth (ψ_s) for a given cycle were constant. Furthermore, since the expected change in aircraft altitude Δh will be small (*e.g.,* 100s of meters) in comparison to the mean cycle altitude $\bar{h}$ (*e.g.,* 10,000 meters), we also assumed that m_{air} was constant over a given cycle. Values of

T_{LK} and G_0 also change slowly. As a result, B could be assumed constant over a given soaring cycle, but was updated across cycles.

IV. AIRCRAFT EQUATIONS OF MOTION

Assume that the aircraft track relative to the air is along the unit vector

$$\mathbf{e}^{\mathrm{V}} = \cos\gamma\sin\psi\mathbf{e}_1 + \cos\gamma\cos\psi\mathbf{e}_2 + \sin\gamma\mathbf{e}_3 \tag{23}$$

where ψ is the heading angle measured clockwise from North, γ is air-relative flight path angle, and $\mathbf{e_1}$ (pointing East), $\mathbf{e_2}$ (pointing North) and $\mathbf{e_3}$ (pointing up) are unit vectors in an earth fixed Cartesian reference frame. The flight trajectory follows the air relative track plus the wind drift,

$$\begin{aligned}\dot{\mathbf{r}} &= \dot{x}\mathbf{e}_1 + \dot{y}\mathbf{e}_2 + \dot{h}\mathbf{e}_3 = V\mathbf{e}^{\mathrm{V}} + \mathbf{W} \\ &= (V\cos\gamma\sin\psi + W_x)\mathbf{e}_1 + V\cos\gamma\cos\psi\mathbf{e}_2 + V\sin\gamma\mathbf{e}_3\end{aligned} \tag{24}$$

where x, y, h are Cartesian coordinates, a dot represents time derivation, and the last equality holds when the wind $\mathbf{W}$ only has an x-component, $W_x(h)$ that depends only on the altitude h. These are the same as Eqs. (9-11) used by Zhao in [11].

Introducing the bank angle μ, and aerodynamic drag parallel and lift perpendicular to the relative wind of the aircraft, into the point mass equations of motion leads to

$$\begin{aligned}m\dot{V} &= -D - mg\sin\gamma - m\dot{W}_x\cos\gamma\sin\psi \\ mV\cos\gamma\dot{\psi} &= L\sin\mu - m\dot{W}_x\cos\psi \\ mV\dot{\gamma} &= L\cos\mu - mg\cos\gamma + m\dot{W}_x\sin\gamma\sin\psi\end{aligned} \tag{25}$$

which are identical to Eqs. (6-8) in [11].

V. TRAJECTORY OPTIMIZATION

A. Generating Feasible Trajectories for Dynamic Soaring

We assume that there exists a constant vertical wind gradient, *i.e.*,

$$\frac{\partial W_x}{\partial h} = \beta \tag{26}$$

where β is a constant. For the general flights where long term travel is disregarded, the equations of motion that need to be solved are

$$\begin{aligned}\dot{V} &= -\frac{D}{m} - g\sin\gamma - \beta V\sin\gamma\cos\gamma\sin\psi \\ \dot{\psi} &= \frac{L\sin\mu}{mV\cos\gamma} - \beta\tan\gamma\cos\psi \\ \dot{\gamma} &= \frac{L\cos\mu}{mV} - \frac{g\cos\gamma}{V} + \beta\sin^2\gamma\sin\psi \\ \dot{h} &= V\sin\gamma\end{aligned} \tag{27}$$

Note the x and y coordinates are not needed and thus omitted; if desired they can be recovered afterwards through integration. Lift L and drag D were assumed to be

$$\begin{aligned}&L = qS_wC_L, \quad C_L^{\min} \le C_L \le C_L^{\max} \\ &D = D_0 + D_i = D_0 + \frac{L^2}{b^2q\pi e}\end{aligned} \tag{28}$$

where S_w is wing planform area, C_L is coefficient of lift, D_0 is from Eq. (7), D_i is induced drag, b is wing span, and e is Oswald's span efficiency factor. If t_f represents the time to complete one cycle, the general optimization problem can be formulated as

$$\max_{C_L,\mu;V,\psi,t_f} \int_0^{t_f} Q\,dt \tag{29}$$

where our objective maximizes a quality function Q subject to the equations of motion constraints in (27), the initial conditions

$$\begin{aligned}&\gamma(0) = 0 \\ &h(0) = h_0\end{aligned} \tag{30}$$

the constraints

$$\begin{aligned}&h \ge h_0 \\ &C_L^{\min} \le C_L \le C_L^{\max} \\ &-\mu_{\max} \le \mu \le \mu_{\max} \\ &-N_{neg} \le \frac{L}{mg} \le N_{pos}\end{aligned} \tag{31}$$

where N_{neg}, N_{pos} are negative and positive load factor limits, and the terminal conditions

$$\begin{aligned}&V(t_f) = V(0) \\ &\psi(t_f) = \psi(0) + 2\pi \\ &\gamma(t_f) = \gamma(0) \\ &h(t_f) \ge h(0)\end{aligned} \tag{32}$$

In other words, at the end of the cycle the aircraft should have the same heading with the airspeed, and at least the same attitude as at the beginning of the cycle. However, it is free to gain altitude. We will provide more information regarding our choice of Q shortly.

As the optimization problem above did not lend itself to an analytical solution, a discrete approximation was used instead. The time for one cycle, t_f, was discretized as

$$t_k = \frac{k-1}{N-1}t_f, \quad k = 1,2,...,N \tag{33}$$

The optimization variables of the discretized version of Eqs. (27-33) can then be written by concatenating the aircraft state variables $\mathbf{x}_k = [V_k, \psi_k, \gamma_k, h_k]^T$ and the control inputs $\mathbf{u}_k = [C_{L,k}, \mu_k]^T$ at each time step with the cycle time, or equivalently

$$\mathbf{X} = \left[V_1, \psi_1, \gamma_1, h_1, C_{L,1}, \mu_1, \ldots, V_N, \psi_N, \gamma_N, h_N, C_{L,N}, \mu_N, t_f\right]^T \tag{34}$$

which has dimension 6N+1.

To ensure the equations of motion in (27) were enforced, they were modeled as non-linear equality constraints. The equations of motion can be written collectively as

$$\dot{\mathbf{x}} = \mathbf{f}(\mathbf{x}, \mathbf{u}) \tag{35}$$

Assume that all functions $\mathbf{x}$ are continuous, continuously differentiable, and cubic within each time interval. Since $\dot{\mathbf{x}} = \mathbf{f}$, the functions $\mathbf{f}$ can be assumed to be quadratic within each time interval. Then $\mathbf{x}_{k+1}$ can be "exactly" calculated from $\mathbf{x}_k$,

$$\begin{aligned} \mathbf{x}_{k+1} &= \mathbf{x}_k + \int_{t_k}^{t_{k+1}} \dot{\mathbf{x}} dt = \mathbf{x}_k + \int_{t_k}^{t_{k+1}} \mathbf{f} dt = \{\text{since } \mathbf{f} \text{ is quadratic}\} \\ &= \mathbf{x}_k + \frac{t_{k+1} - t_k}{6}\left(\mathbf{f}_{k+1} + 4\mathbf{f}_{m,k} + \mathbf{f}_k\right) \end{aligned} \tag{36}$$

where $\mathbf{f}_{m,k}$ is the value of $\mathbf{f}$ at the midpoint between t_k and t_{k+1}. The midpoint value of $\mathbf{f}$ can be obtained by inserting midpoint values of $\mathbf{x}$ and $\mathbf{u}$ into the known function $\mathbf{f}$. The midpoint value $\mathbf{x}_{m,k}$ is obtained from the fact that $\mathbf{x}$ was assumed to be cubic and from the endpoint values $\mathbf{x}_k, \mathbf{x}_{k+1}, \dot{\mathbf{x}}_k = \mathbf{f}_k, \dot{\mathbf{x}}_{k+1} = \mathbf{f}_{k+1}$

$$\mathbf{x}_{m,k} = \frac{1}{2}\left(\mathbf{x}_{k+1} + \mathbf{x}_k\right) + \frac{t_{k+1} - t_k}{8}\left(\mathbf{f}_k - \mathbf{f}_{k+1}\right) \tag{37}$$

If the control $\mathbf{u}$ is assumed to be linear within each time interval, then the midpoint value of the control is simply

$$\mathbf{u}_{m,k} = \frac{1}{2}\left(\mathbf{u}_{k+1} + \mathbf{u}_k\right) \tag{38}$$

Thus the motion constraints can be expressed solely in terms of the optimization variables at each time-step. The net result is that feasible dynamic soaring trajectories can be defined by constraints on the initial and terminal trajectory conditions, as well as constraints on the aircraft state and control inputs at each time step.

B. Determining a Feasible Aircraft Design

In Section V.A, we showed that a feasible, perpetual soaring trajectory can be modeled through non-linear constraints on the aircraft state and control inputs. We now extend these results to solve for our aircraft design variables. In doing so, we augment (34) with four additional parameters

$$\mathbf{X} = \left[\mathbf{x}_1, \mathbf{u}_1, \ldots, \mathbf{x}_N, \mathbf{u}_N, t_f, S_w, b, l, m\right]^T \tag{39}$$

corresponding to the aircraft wing area, wingspan, fuselage length, and mass, respectively. Note that the drag associated with our aircraft design in (7) has already been integrated into (28). Thus, we need only augment our constraint set with (4) and (18) to account for lower bounds on b and m, respectively, for an aircraft design capable of maintaining perpetual flight in a given wind gradient β. Note in practice, additional constraints on the aircraft design parameters could readily be added to stay within a desired range of aircraft geometries.

To recover the aircraft design parameters, we must still define a suitable quality function Q. In this work, we define our objective function as

$$\min_{S_w, b, l, m} \frac{1}{N}\sum_{k=1}^{N} V_k \tag{40}$$

In other words, our aircraft design will be capable of maintaining a perpetual dynamic soaring cycle at the lowest average velocity possible. The motivation for this is that less efficient soaring cycles that optimize an alternate quality function (*e.g.,* solar power generation) would still be feasible at higher aircraft velocities. Note that alternate objective functions could be imagined that are equally good.

To summarize, by solving the constrained optimization problem at (40), we will be obtain a locally optimal set of design parameters $\{S_w^*, b^*, l^*, m^*\}$ for our aircraft model

C. Trajectories for Optimizing Solar Power Generation

To this point, we have developed an approach to determine aircraft design parameters suitable for dynamic soaring. Given such an aircraft, our objective is to generate efficient trajectories for optimizing solar power generation. We assume that the aircraft has a solar cell array integrated into the top wing surface in order to generate electric power. The task presently considered is to develop an optimal periodic flight trajectory that enables the maximum amount of energy to be extracted from the solar cells without the airplane losing altitude. Further constraints on aircraft long term traveling direction and speed, including loitering (no travel), could also be imposed but were presently ignored.

To solve this task, we revert back to our initial problem formulation from Section V.A using the recovered aircraft design parameters $\{S_w^*, b^*, l^*, m^*\}$ which are no longer optimization variables. We redefine the objective function in (29) as

$$\max_{c_L, \mu, V, \psi, t_f} \frac{\eta_c A_c B}{N}\sum_{k=1}^{N} \max\left(\hat{u}_c^T \hat{u}_S, 0\right) \tag{41}$$

where η_c represents the solar cell efficiency, A_c the area of the solar cell aray, and B the beam irradiance from (19). The summand is the dot product of the unit normal of the solar cell array $\hat{u_c}$ with the unit vector $\hat{u_S}$ corresponding to the direction to the sun (both with respect to the earth frame), or equivalently the cosine of the solar incidence angle between the sun and the solar cell array. Note the *max* function is necessitated by the dot product being negative when the solar cell is oriented in the opposite direction to the sun. This geometry would correspond to zero (*not* negative) generated power since we assume the solar cells are only mounted on the top of the wing. The net result is that for a given aircraft design, the solution to Eq. (41) will yield a locally optimal periodic trajectory for a dynamic soaring aircraft which maximizes the amount of power generated from an onboard solar cell array.

VI. SIMULATION RESULTS

In an attempt to validate our approach, the aircraft design and solar power generation sub-problems were solved in simulation using a non-linear programming solver. We examined "worst case" conditions for solar power generation corresponding to the winter solstice (21 Dec) in the northern hemisphere. The simulated test location was at 30° latitude, which is representative of the southerly limit of the northern hemisphere polar jet stream in winter. The Linke turbidity factor for the atmosphere at this latitude was estimated as T_{LK}= 3.0 based upon [17].

For all trials, we assumed a vertical wind gradient β=0.01 s^{-1} with winds from the west (-x direction), and the trajectory discretization resolution was N=60 steps. The aircraft design parameters used in solving Eq. (41) were b=2.50 m, S_w =0.40 m^2, l=1.50 m, and m= 41.5 kg. These were obtained from solving the objective function in Eq. (40).

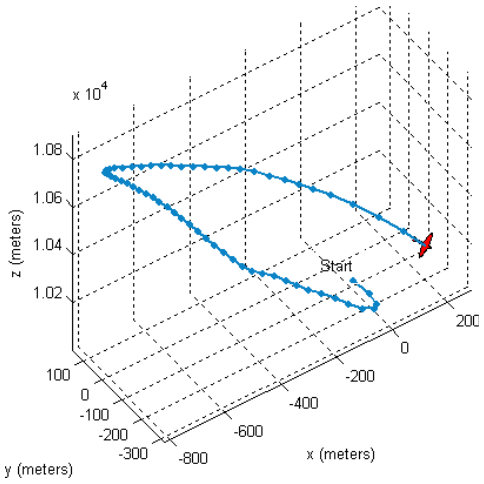

Figure 2: Dynamic soaring trajectories for optimizing solar exposure at sunrise.

Representative results for a trajectory that optimized solar power generation at sunrise are shown at Figure 2. As is characteristic of dynamic soaring cycles, the aircraft climbed into the wind and dove with the wind, exchanging velocity for altitude. This is clearly illustrated in Figure 3, which shows the aircraft velocity (top) and altitude vs. time.

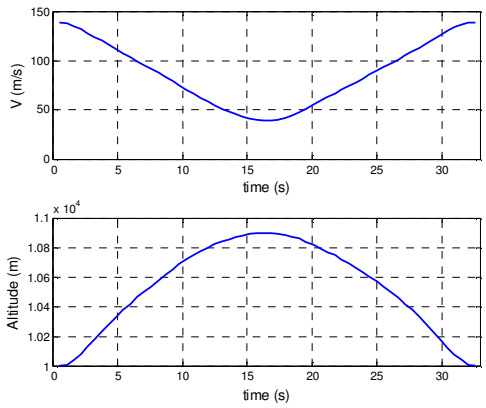

Figure 3: Aircraft velocity (top) and altitude (bottom) vs. time for the sunrise trajectory. The exchange of velocity for altitude is characteristic of the dynamic soaring cycle.

In contrast, Figure 4 shows a trajectory that optimizes solar power generation at midday. While the trajectories in both Figure 2 and Figure 4 satisfy our constraints for periodic soaring cycles, they are dramatically different. This is a result of the significant differences in solar altitude and azimuth vs. the time of day. This effect is further reinforced by Figure 5, which shows the power generated vs.. time of day for 21 different trajectories generated at 30 minute intervals. These assume a solar cell efficiency η_c = 0.4, and a solar cell area A_c=*0.9*S_w.

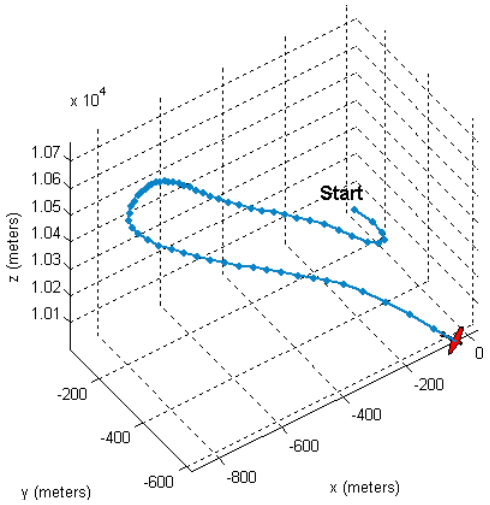

Figure 4: Dynamic soaring trajectories for optimizing solar exposure at midday. Note that minimizing the aircraft incidence angle to the sun results in a dramatically different trajectory to the sunrise mission due to significant changes in the solar altitude/azimuth.

The upper solid blue line in Figure 5 shows the average generated power vs. time from our optimized solar trajectory using the objective function at Eq. (41). In contrast, the lower dotted red line shows the average power generated when the aircraft follows the minimum velocity cycle specified by Eq. (40). Observe that in both cases, the power generated is not symmetric, as one might initially suspect. This is due to the westerly wind direction, which generally implies a soaring strategy of climbing into the west, and then diving when turning east. The net result is a bias in the amount of solar exposure when the sun is in the eastern sky, which is reflected in Figure 5 for both cases. However, the power generated for the two soaring strategies is dramatically different. For the minimum velocity cycle, the average power generated over the 24 hour period was 16.1 watts. In contrast, the average power generated for the optimized solar cycle was 32.6 watts. This more than doubling of the generated power demonstrates the efficacy of our optimization approach. Furthermore, when considering that autopilot systems such as the Piccolo II consume about 4 watts [22], this power level appears to be sufficient for aircraft control and communications requirements.

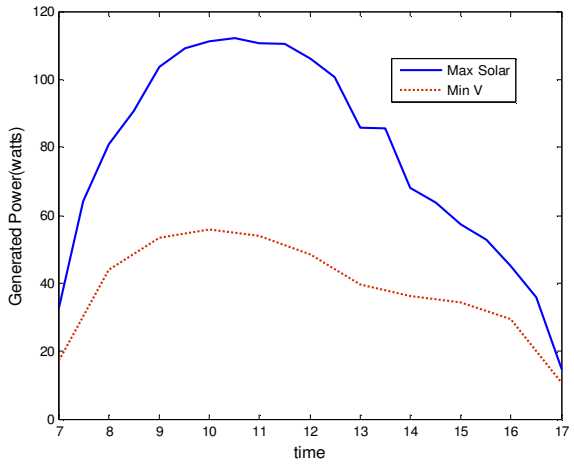

Figure 3: Power generated vs. time of day for trajectories optimizing velocity (bottom) vs. solar power (top). The average power generated over the 24 hour period was 16.1 and 32.6 watts, respectively.

VII. DISCUSSION

This work represents our initial efforts to develop an unmanned aerial vehicle capable of perpetual flight in the jet stream. We investigated both the aircraft design requirements necessary for unpowered flight in representative wind gradients, as well as trajectories for generating solar power for on-board avionics and control systems. Simulation results indicate the feasibility of perpetual flight in jet stream level wind gradients. This is of course just a small initial step. We are beginning to evaluate different aircraft designs using a Piccolo SL autopilot in order to demonstrate autonomous dynamic soaring on an actual aircraft. For on-board power generation, we are also evaluating the feasibility of a Ram Air Turbine (RAT) as an alternate to solar. An advantage of the RAT is it can provide continuous power regardless of time of day, and reduce the battery storage requirements associated with solar power generation.

ACKNOWLEDGMENT

The research was supported by the Office of Vice President and Associate Provost for Research and Graduate Studies, the P.C. Rossin College of Engineering and Applied Science, the Department of Mechanical Engineering and Mechanics, and the Department of Computer Science and Engineering, Lehigh University.

REFERENCES

[1] Kyle, E., "2009 Space Launch Report," 30 Dec 2009, http://www.spacelaunchreport.com/log2009.html

[2] R. J. Boucher, "History of Solar Flight," in *Proc. of the 20th Joint Propulsion Conference, AIAA-84-1429*, Cincinnati, USA, June 1984

[3] "AC Propulsion's Solar Electric Powered SoLong UAV," AC Propulsion Report, San Dimas, CA June 2005

[4] Noth, A., Engel, W., Siegwart, R.,"Flying Solo and Solar to Mars - Global Design of a Solar Autonomous Airplane for Sustainable Flight", IEEE Robotics and Automation Magazine, Vol. 13, No. 3, September 2006

[5] A. Klesh and T. Kabamba , "Solar-powered Aircraft: Energy-Optimal Path Planning and Perpetual Endurance," Journal of Guidance, Control and Dynamics, Vol. 32, No. 4, Jul-Aug 2009

[6] Vulture Program, Defense Advanced Research Projects Agency, http://www.darpa.mil/news_images/vulture-02.html

[7] "Solar Impulse – Around the World in a Solar Airplane," http://www.solarimpulse.com/

[8] Rayleigh, J.W.S., "The Soaring of Birds," Nature, 27, 534-535, 1883.

[9] Cone, C.D., Jr., "A mathematical analysis of the dynamic soaring flight of the albatross with ecological interpretations," Virginia Institute of Marine Science Special Scientific Report. No. 50, pp. 104, 1964.

[10] Boslough, Mark B.E. Autonomous dynamic soaring Platform for Distributed Mobile Sensor Arrays, SAND2002-1896, Sandia National Laboratories, Albuquerque, NM, 2002.

[11] Zhao, Y.J., "Optimal Patterns of Glider Dynamic Soaring," Optimal Control Applications and Methods, Vol. 25, No. 2, pp. 67-89., 2004.

[12] Sachs, G., da Costa, O., "Periodic Optimal Control for Dynamic Soaring in the Shear Wind Associated with Jet Streams," ICNPAA-2006: Mathematical Problems in Engineering and Aerospace Sciences, Budapest University of Technology and Economics, Budapest, Hungary, June 21-23, 2006.

[13] Gordon, R.J., "Optimal dynamic soaring for full size sailplanes," M.Sc. Thesis, Air Force Institute of Technology, Wright-Patterson Air Force Base, Ohio, 2006.

[14] Akhtar, N., Whidborne, J., and Cooke, A., "Real-time trajjecotry generation technique for dynamic soaring UAVs," International Conference on Control, Manchester, U.K., Sep 2008

[15] Lawrance, N. and Sukkarieh, S., "A Guidance and Control Strategy for Dynamic Soaring with a Gliding UAV," in Proceedings of the International Conference on Robotics and Automation, Kobe, Japan, May 2009

[16] Lawrance, N. and Sukkarieh, S., "Wind Energy Based Path Planning for a Small Gliding Unmanned Aerial Vechicle," in AIAA Guidance, Navigation, and Control Conference, Chicago, USA, Aug 2009

[17] Remund J., Wald L., Lefevre M., Ranchin T., Page J., "Worldwide Linke turbidity information," in the Proceedings of ISES Solar World Congress, 16-19 June 2003, Göteborg, Sweden

[18] Page, J., Albuisson, M., Wald, L., "The European solar radiation atlas: a valuable digital tool," Solar Energy, 71, 2001, pp. 81-83

[19] Rigollier, Ch., Bauer, O., Wald, L. , "On the clear sky model of the ESRA - European Solar radiation Atlas - with respect to the Heliosat method," Solar energy, 68, 2000, pp. 33-48

[20] Scharmer, K., Greif, J., eds., "The European solar radiation atlas, Vol. 2: Database and exploitation software," Paris (Les Presses de l' École des Mines), 2000

[21] Hofierka J., Šúri M., **"**The solar radiation model for Open source GIS: implementation and applications," in Ciolli M., Zatelli P. (Eds.), Proceeding of conference "Open source GIS - GRASS users conference 2002", Trento (Italy), Sep 2002

[22] "Piccolo II Data Sheet," Cloud Cap Technology, Hood River, OR, Sep 2009

[23] "The Jet Stream," National Weather Service, http://www.srh.noaa.gov/jetstream//global/jet.htm, accessed Mar 2010

[24] Hopkins, E., "Charts for Predicting Turbulent Skin Friction From the Van Driest Method," NASA TN D-6945, Ames Research Center, Oct 1972

[25] Deittert, M., Toomer, C., and Pipe, A., "Engineless Unmanned Aerial Vehicle Propulsion and Dynamic Soaring," in the Journal of Guidance, Control, and Dynamics, Vol. 32, No. 5, Sep-Oct 2009